PCCP

ROYAL SOCIETY OF CHEMISTRY

PAPER

View Article Online
View Journal | View Issue

Cite this: *Phys. Chem. Chem. Phys.*, 2024, **26**, 12619

Unveiling the quantum secrets of triel metal triangles: a tale of stability, aromaticity, and relativistic effects†

Sílvia Escayola, [ab] Elisa Jimenez-Izal, [bc] Eduard Matito, [bd] Jesus M. Ugalde, [bc] Rafael Grande-Aztatzi *[be] and Jose M. Mercero *[bc]

Low lying electronic states of Al_3^-, Ga_3^-, In_3^-, and Tl_3^- have been characterized using high level multiconfigurational quasi degenerate perturbation theory on the multiconfigurational self-consistent field. Among these species, the singlet $^1A_1''$ states emerge as the predominant energy minima, displaying remarkable stability. However, within the Tl_3^- series, our investigation leads to the identification of the high-spin $^5A_1''$, as the most stable spin state, a result corroborated by previous experimental detection *via* photoelectron spectroscopy. Similarly, we have also identified the singlet state of In_3^- as the signal detected previously experimentally. By applying Mandado's rules and an array of aromaticity indicators, it is conclusively demonstrated that both the singlet and quintet states exhibit multiple-fold aromaticity, while the triplets exhibit conflicting aromaticity. Furthermore, this investigation highlights the significant impact of relativistic effects, as they enhance the stability of the $^5A_2''$-Tl_3^- state relative to its singlet counterpart. These findings shed new light on the electronic structures and properties of these ions, offering valuable insights into their chemical behavior and potential applications.

Received 1st February 2024,
Accepted 22nd March 2024

DOI: 10.1039/d4cp00484a

rsc.li/pccp

1 Introduction

Al_3 triangles have widely been studied theoretically and experimentally, in both the ground state and excited states.[1–10] However, its anionic form Al_3^- has been studied to a lesser extent. The first study of Al_3^- we have found in the literature was conducted by H. Basch.[1] He calculated the electronic properties of the anion using MCSCF methods, and a C_{2v} symmetry triangle was reported as the ground state. Later, Taylor *et al.* and Ganteför *et al.* studied Al_3^- using photoelectron spectroscopy.[11,12] In 1995, Calaminici *et al.*[2] reported a D_{3h} triangle as the singlet ground state using DFT. In 1998, Baeck and Bartlet[3] characterized the low-lying electronic states of Al_3^- using the CCSD(T), confirming an equilateral triangle as the ground state $\left(^1A_1'\right)$.

A few years later, Kuznetsov and Boldyrev[13] extended the all-metal aromaticity concept to the Al_3^- and Ga_3^- anions, describing both triangles as π-aromatic systems. Later on, Zhan *et al.* pointed out that the Al_3^- triangle was not just π-aromatic,[14] and introduced the idea of multiple-fold aromaticity, showing a two-fold aromatic system, π- and σ-aromatic. In 2009, Villalta and Leopold,[5] experimentally characterized both the ground and excited states of Al_3 and Al_3^- trimers, confirming the $^1A_1'$ state as the ground state. These experimental results were rationalized with single-reference DFT and coupled cluster methods by Miller *et al.*[4]

In 2015, we described the lowest-lying electronic states of the Al_3^- triangle using DFT and multiconfigurational high-level calculations supplemented with quasi-degenerated perturbation theory.[15] We showed that not only the ground state, but the triplet and quintet excited states were aromatic. Recently, Al_3^- aromaticity was analyzed by means of the natural orbital functional (NOF) theory.[16]

Ga_3, In_3, and Tl_3 trimers have also been previoulsy studied. Pöttgen and coworkers have characterized many crystal structures where Al_3,[17] Ga_3,[18–21] and In_3,[22–24] triangles are present, and there are many other similar structures reported in the literature.[25–27] Some molecules where Ga_3 triangles are identified have also been synthesized.[28–31] Theoretical investigations are also available for Ga_3 and In_3 in the literature.[32–38] Among all these studies, only a few have focused on triangular anions.

[a] *Institute of Computational Chemistry and Catalysis and Department of Chemistry, University of Girona, C/M. Aurèlia Capmany, 69, 17003 Girona, Catalonia, Spain*
[b] *Donostia International Physics Center (DIPC), 20018 Donostia, Euskadi, Spain. E-mail: aztatzi26@gmail.com, jm.mercero@ehu.eus*
[c] *Kimika Fakultatea, Euskal Herriko Unibertsitatea (UPV/EHU), P.K. 1072, 20080 Donostia, Euskadi, Spain*
[d] *IKERBASQUE, Basque Foundation for Science, 48013 Bilbao, Euskadi, Spain*
[e] *Escuela de Ingeniería y Ciencias, Tecnológico de Monterrey, Av. Eugenio Garza Sada 2501, 64849 Monterrey, Nuevo León, Mexico*

† Electronic supplementary information (ESI) available. See DOI: https://doi.org/10.1039/d4cp00484a

In 1990, Meier *et al.*[33] studied Ga_3^- using MRD-CI techniques; few years later, in 1994, Cha *et al.*[39] obtained the photoelectron spectra for Ga_3^-. In 2002, Kuznetsov and Boldyrev,[13] described the aromaticity of the Ga_3^-. There is a limited number of research works dedicated to the investigation of In_3^-. Gausa *et al.* performed photoelectron spectroscopy experiments for In_n^- and Tl_n^- clusters.[36] The studies regarding the Tl_3 are scarce, including those by Gausa *et al.* and Vijayakumar *et al.*,[40] who used MCSCF methods to characterize $Tl_3^{+/-}$ molecules, while Kang[41] described the Tl_3^+ triangle in 1993, and Tsipis *et al.* discussed NICS evolution in different compounds including the Tl_3^-.[42]

The manuscript at hand employees multiconfigurational self-consistent methods to investigate X_3^- triangles, (where X= Al, Ga, In, and Tl), exploring several properties of the lowest-energy spin states. The study establishes a connection between the experimentally measured photoelectron spectra and the $^1A_1'$ state of In_3^- and $^5A_2''$ state of Tl_3^-. Additionally, the aromaticity of the complexes is analyzed using the multicenter index (MCI) and its π-fraction (MCI_π) across different electronic configurations to demonstrate the multiple-fold aromaticity determined by the independent delocalized σ and π bonding systems. The study also employs delocalization indexes[43,44] (DI) and adaptive natural density partitioning analysis[45] (AdNDP) to obtain an alternative perspective and quantify the aromaticity, and finally, a magnetic criteria is also used, the iso-chemical-shielding surfaces[46,47] (ICSS) method.

2 Methods

State-specific multiconfigurational self consistent field (MCSCF)[48] complemented by multiconfigurational quasi-degenerate perturbation (MCQDPT)[49] methods have been employed to characterize the electronic structure of the different X_3^- (X= Al, Ga, In and Tl) triangles by using the Karlsruhe Def2-TZVPPD[50,51] basis set wich includes pseudopotentials for In[52] and Tl.[53] Inconsistencies caused by the so-called intruder states, which appear when the perturbation expansion of the reference MCSCF wave function has vanishingly small energy denominators, were remedied by shifting them by 0.02 a.u., as recommended earlier.[54] The vibrational frequencies were also calculated at the MCSCF level of theory. The ten valence electrons of the system were included in the active space, which were allowed to distribute themselves in twelve molecular orbitals (MO) (full active space). The selected twelve orbitals are the ones depicted in Fig. 1 and encompass the different-fold aromatic systems as described with elegant simplicity by Dixon *et al.*[14] spin–orbit coupling where estimated using the Pauli–Breit approximation for the coupling Hamiltonian, at the aforementioned level of theory as implemented in the GAMESS US program.[55]

The aromaticity of the characterized triangular systems has been assessed by means of different analysis tools, multicenter index (MCI),[56] adaptive natural density partitioning (AdNDP)[45] and the iso-chemical-shielding surfaces (ICSS) method.[46,47] Although these tools are all used to measure the aromaticity in molecules, they differ in their methods. MCI quantifies the degree of magnetic circuit delocalization in a molecule by integrating the magnetic flux density along a closed loop that passes through the aromatic ring, AdNDP uses a natural orbital-based partitioning scheme to analyze electron density by partitioning it into natural orbitals. In conclusion, these methods can be used together to provide a more comprehensive understanding of the electron delocalization in a molecule. MCI and DI have been calculated using the ESI-3D program,[44,57] and were computed for all the isomers using their corresponding MCSCF (10,12) wave functions. The atomic overlap matrices, required by ESI-3D to calculate the MCIs, were obtained from the APOST-3D[58] software using the topological fuzzy Voronoi (TVFC) cell partition.[59–61] To account for the numerical errors in APOST-3D and ESI-3D, we verified that the number of electrons was equal to the sum of all the electron populations of the molecule, the error being always below 0.0016 a.u.

AdNDP and ICSS analysis were carried out at the CAM-B3LYP/Def2-TZVPP level of theory. ICSS method was used *via* Multiwfn code.[62]

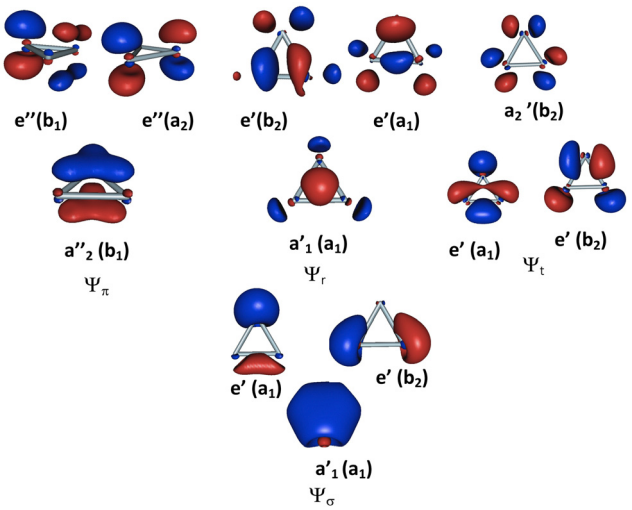

Fig. 1 MCSCF(10,12) natural orbitals (NOs) of the Al_3^- grouped in the four aromatic independent systems, Ψ_σ, Ψ_π, Ψ_r and Ψ_t, σ, π, radial and tangential, respectively. The orbitals for the singlet and the quintet are similar, while, despite of the symmetry change to C_{2v}, the triplet structures triangles maintain a similar form (C_{2v} symmetry equivalent labels are given in parentheses).

3 Results

In this manuscript, we will explore the various properties of the lowest-energy spin states, namely, $^1A_1'$, $^3B_2$ and $^5A_2''$, of the X_3^- (where X = Al, Ga, In, and Tl) triangles. The geometries of these structures were optimized at the MCSCF (10,12) level, and their energies were refined at the MCQDPT level of theory. Our results exhibit a substantial multireference character for these structures. The $^1A_1'$ ground states are mainly dominated by the $(a_2'')^2(a_1')^2$ single reference state (with a configuration

interaction coefficient (CIC) of around 0.9, see Table S3 in ESI† for the main CICs of the different molecules states), with significant contributions from each of the two configurations featuring degenerate orbitals $(a_2'')^2(e')^2$ and $(a_1')^2(e')^2$, both with identical CIC coefficients (note that the other six electrons are in the Ψ_σ system, see Fig. 1). The $^3B_2$ states main configuration is the $(b_1)^2(a_1)^1(b_2)^1$ with a CIC around 0.88. Lastly, the quintets exhibit the smallest multiconfigurational character, with the $(a_2'')^1(a_1')^1(e')^1(e')^1$ configuration being dominant, with a CIC around 0.92.

As previously reported in the literature,[63,64] the aluminum trimers possess four independent MO sets derived from the s-type and p-type atomic orbitals (AO) (Fig. 1). The Ψ_σ set is formed by the three s-AOs, the three p_z-AOs form the Ψ_π, the p orbitals oriented in the radial direction form the Ψ_r (radial) set, and p-orbitals oriented in the tangential direction the Ψ_t (tangential) (see Fig. 1). These group-13 X_3^- triangles possess a valence shell of ten electrons, six of which are located in the Ψ_σ orbitals, and the remaining four are arranged in four orbitals with similar energies. We observed the same MO sets in all the complexes studied.

Table 1 presents a summary of the geometrical, energetic, and aromaticity properties obtained for the lowest-lying energy spin-states of the X_3^- (X = Al, Ga, In and Tl) triangles. The $^3A_1$, $^3A_2$, and $^3B_1$ states were also characterized, but they were found to be higher in energy than the $^3B_2$, and in the interest of brevity, we will focus only on the lowest state, although the details of the $^3A_1$, $^3A_2$, and $^3B_1$ states can be found in the ESI† (see Table S1).

Table 1 Calculated properties of the lowest-energy spin-states of the X_3^- triangles (where X = Al, Ga, In, and Tl). Symm. stands for the symmetry of the molecule, the values of ΔE are ZPE-corrected MCQDP/MCSCF (10,12) relative energies, expressed in kcal mol^{-1} with respect to the singlet state. R represents the equilibrium bond lengths of the triangles in Å. Note that 1, 2, and 3 refer to the atom numbers, so $R_{1,2}^{1,3}$ means that the bond length between atoms 1 and 2, and 1 and 3 is the same, and $R_{2,3}$ corresponds to the distance between atoms 2 and 3. This situation corresponds to C_{2v} symmetry. However, it is important to recall that for D_{3h} molecules, ($R_{1,2}^{1,3}$) and $R_{2,3}$ are equal. The same applies to δ, the atom-pair (determined by the sub and super indexes) DI, where, in the triplets, $\delta_{1,3}^{1,2}$ stands for the equal-size atom-pair DI, and $\delta_{2,3}$ to the longer size atom-pair. The total multi-center index (MCI) is also reported along with its π contribution to the aromaticity (MCI_π)

M	Symm.	ΔE	$R_{1,3}^{1,2}$	$R_{2,3}$	MCI	MCI_π	$\delta(X_3^-)$	$\delta_{1,2}^{1,3}$	$\delta_{2,3}$
Al_3^-									
$^1A_1'$	D_{3h}	0.0	2.558		0.48	0.23	3.11	1.07	
$^3B_2$	C_{2v}	7.36	2.543	2.762	0.35	0.22	2.95	1.00	0.92
$^5A_2''$	D_{3h}	12.18	2.758		0.12	0.03	2.46	0.82	
Ga_3^-									
$^1A_1'$	D_{3h}	0.0	2.576		0.48	0.24	3.01	1.00	
$^3B_2$	C_{2v}	7.04	2.552	2.835	0.35	0.23	2.81	1.05	0.72
$^5A_2''$	D_{3h}	11.93	2.777		0.11	0.03	2.29	0.80	
In_3^-									
$^1A_1'$	D_{3h}	0.0	2.979		0.47	0.22	2.86	0.96	
$^3B_2$	C_{2v}	2.54	2.931	3.326	0.32	0.22	2.71	1.01	0.69
$^5A_2''$	D_{3h}	3.20	3.147		0.10	0.03	2.35	0.78	
Tl_3^-									
$^1A_1'$	D_{3h}	0.0	3.129		0.46	0.22	2.68	0.89	
$^3B_2$	C_{2v}	−0.71	3.049	3.441	0.29	0.22	2.56	0.97	0.63
$^5A_2''$	D_{3h}	−2.94	3.263		0.08	0.03	2.30	0.77	

Upon analyzing the outcomes, it is evident that Al_3^- and Ga_3^- not only have a similar size but also exhibit comparable energy differences between different electronic states. Specifically, there is a difference of approximately 7 kcal mol^{-1} in energy for the $^3B_2$ state and 12 kcal mol^{-1} for the $^5A_2''$ state, with respect to the singlets. Conversely, the In_3^- ion is found to be significantly larger in size, and the energy differences between electronic states are reduced to 2.54 and 3.20 kcal mol^{-1} for the triplet and quintet states with respect to the singlet. Importantly, for Tl_3^-, the picture changes, with the quintet being the most stable electronic state followed by the triplet and the singlet, which are around 2.2 and 2.9 kcal mol^{-1} higher in energy, respectively. Additionally, spin–orbit couplings were measured and found to be small, smaller than 5 cm^{-1}.

Intrigued by the fact that the quintet spin state is the most stable electronic state of Tl_3^-, vertical detachment energy (VDE) energy calculations were performed to compare them with the photoelectron spectrum reported by Gausa *et al.*[36] Such spectrum exhibited three primary signals, one at 1.5 eV, another at 1.7 eV, and the third around 2.2 eV. We conducted MCQDPT VDE calculations beginning from the $^5A_1$ state, which yielded two degenerated VDEs of 1.30 eV, corresponding to detachment of the e′ electrons, another of 1.66 eV for the detachment of the a_2'' electron, and the fourth of 1.77 eV for the a_1' electron. We also performed partial third-order quasiparticle theory[65] (P3) electron propagator calculations (as implemented in Gaussian 16[66]), which resulted in VDEs of 1.52, 1.76, and 2.12 eV for the quintet, corresponding to e′, a_2'', and a_1' electron detachments, respectively. Based on our calculations, we can conclude that the experimentally detected signal corresponds to the quintet electronic state of the Tl_3^- molecule.

We also calculated the VDE's for In_3^- and compared it to the photoelectron spectrum measured by Gausa *et al.*[36] The experimental spectrum exhibited two primary signals, one around 1.65 eV and the other around 1.85 eV. Our MCQDPT calculations resulted in VDEs of 1.70 eV and 1.74 eV, which are consistent with the experimentally measured signals. Additionally, using the Partial Third-order quasiparticle theory[65] (P3) electron propagator, we obtained VDEs of 1.69 eV and 1.85 eV, in excellent agreement with the experimental signals. Therefore, it is inferred that the detected signals correspond to the $^1A_1'$ electronic state of In_3^-.

The results for Al_3^- and Ga_3^- are consistent with previous theoretical and experimental findings. Villalta *et al.* experimentally identified a triplet excited state with an obtuse (C_{2v} symmetry) triangle geometry, $^3B_2$ electronic configuration and 9.43 kcal mol^{-1} higher in energy than the singlet state. Two sides of the triangle have equal lengths, similar to those of the ground state, while the third side is 0.187 Å larger. Our high-level *ab initio* calculations, as shown in Table 1, are in excellent agreement with their experimental results.[5]

Note that our calculations indicate highly correlated electronic structures for all the systems considered. However, there is

excellent agreement between our results and those obtained from DFT/CCSD(T)[4] and CCSD(T)[3] calculations, as well as with experimental counterparts.[5]

It is noteworthy that the quintet state is the most stable electronic state for Tl_3^-, which is in contrast to the well-studied case of Al_3^-, where the singlet state is the most stable and exhibits the highest aromaticity when compared with the $^3B_2$ and $^5A_2''$ states. We have analyzed the aromaticity of Tl_3^- and compared it with that of the Al_3^- triangle, to unveil its effect on the stability of the Tl_3^-.

Aromaticity is a concept that lacks a precise definition and does not correspond to any measurable physical property. As a result, it is difficult to identify a specific property that can determine aromaticity.[67–69] To address this challenge, numerous indicators have been developed, including the multicenter index (MCI)[56] and the I_{ring}[70] multicenter index, which are among the most reliable indicators for small systems,[71] and are also valid for analyzing metalloaromaticity.[72] For triangular systems, it is important to note that the MCI and I_{ring} values are equivalent. In such cases, the MCI and I_{ring} values measure the degree of simultaneous electron sharing between different centers and can be used to estimate aromaticity.

To compare the aromaticity of different rings, MCI value needs to be normalized to the number of atoms (n), $MCI^{1/n}$, as MCI is known to be dependent on ring size.[73,74] The normalized $MCI^{1/3}$ value for benzene is 0.65 e, (obtained using CAM-B3LYP/6-311G(d,p)[75]). For Al_3^-, the normalized MCI value is larger, 0.85 e, while the inclusion of electron correlation reduces the $MCI^{1/3}$ value to 0.79. Therefore, it is clear that these triangles are aromatic. As we will be working with molecules of the same size, we will focus on the MCI indices, see Table 1. When analyzing them, we observe large values for both the singlet and triplets, whereas the MCI values of the quintets are comparatively lower but not negligible, *i.e.*, $MCI^{1/3}$ are 0.49 and 0.43 for Al_3^- and Tl_3^- respectively.

To better understand the origin of aromaticity, we looked at the π and σ-aromaticities separately, (see MCI_π in Table 1, and note that $MCI_{\sigma_T} = MCI - MCI_\pi$). While the origin of the π-aromaticity is directly linked with the Ψ_π MOs set, the σ_T-aromaticity (σ total aromaticity) can arise from the other three different sets, Ψ_σ, Ψ_r, and Ψ_t, shown in Fig. 1. We found that in the $^1A_1'$ ground states, MCI_{σ_T} was slightly larger than MCI_π. In the $^3B_2$ states, an electron was excited from the radial a_1' NO, to the tangential b_2, resulting in a reduction of MCI_{σ_T}, with values ranging from 0.07 *e* for Tl_3^- to 0.13 *e* for Al_3^-. In the quintets, another electron is excited from the π a_2'' NO to the second degenerate tangential NO, leaving the a_2'', a_2' and both e′ MOs singly occupied. As a result, both MCI_π and MCI_{σ_T} were reduced (see Table 1).

Together with the MCI, DI can help us construct a vision of the electronic structure of the system. In Table 1, the total DI $\delta(X_3^-)$ are shown. These numbers give us an estimation of the number of electron pairs delocalized in the system. According to these indexes, the delocalization is significant, very large in the singlets, and smaller for the triplets and quintets. The $\delta(X_3^-)$ indexes for the quintets are noteworthy, ranging from 2.46 for Al_3^- to 2.30 for the Tl_3^-. For the D_{3h} symmetry states, the properties of the three bonds are equal, so are the atom-pair DI, however for the C_{2v} symmetry triplets, we have two long and one short bonds with different atom-pair DI as it can be seen in Table 1.

In order to gain a deeper understanding of the origin of the DI, we have separated the contribution of each molecular orbital sets (described in Fig. 1) to the atom-pair DI. The resulting figures are collected in Table 2 (note that for the sake of brevity the two extreme cases are shown, Ga_3^- and In_3^- data is summarized in the ESI,† see Table S2). An examination of the $^1A_1''$-Al_3^- DIs, describe that 1.5 electron-pairs (0.48 × 3) are delocalized in the Ψ_σ set, alongside two delocalized electron pairs one in the π- and the second in the r-set. The main difference for the Tl_3^- is the reduction of the delocalization of the Ψ_σ set. In the context of triplets, the delocalization of the Ψ_σ and Ψ_π sets is very similar to that of the singlet states, while the delocalization of the radial set reduces to 0.24 electron-pairs with a simultaneous increase in the delocalization of the Ψ_t-set. This behavior is what we could expect since an electron from the Ψ_r-set is excited to one of the Ψ_t sets. Finally, in the $^5A_2''$ states, Ψ_π-delocalization is also reduced and Ψ_t DI increases again as a consequence of the excitation of one of the π-electrons to the second Ψ_t tangential set.

The adaptive natural density partitioning analysis (AdNDP) method[45] has also been applied to our molecules. AdNDP localizes the valence electrons in 1-center 2-electron bonds (1c–2e), 2-center 2-electron bonds (2c–2e) and n-center 2-electron bonds (nc–2e). For the singlet states, AdNDP produces three possible bonding pictures, as shown in Fig. 2. The first one consists of three lone pairs (occupation numbers, ON = 1.78 |e|), and two 3c–2e bonds (ON = 1.99 |e|) of σ and π nature. An analogous picture is obtained instead by localizing the electronic density into 2c–2e bonds (ON = 1.99) along with the same two 3c–2e bonds (ON = 1.99 |e|). Lastly, the electronic density can be fully delocalized into 3c–2e bonds (ON = 1.99 |e|) (see Fig. 2C). These five 3c–2e AdNDP bonds and the a_1', e′, e′ (of the Ψ_σ set), the a_2'' (of the Ψ_π set) and a_1' (of the Ψ_r set) natural orbitals shown in Fig. 1 are similar in shape. The latter description is in agreement with the high delocalization found in these molecules. The co-existence of the two alter-

Table 2 Contribution of the different MO sets (see Fig. 1) to the atom-pair DIs for the Al_3^- and Tl_3^- different electronic states. The first values of the triplet correspond to the symmetric atom-pair corresponding to the two short bonds while the second corresponds the atom-pairs forming the longest bond

	Al_3^-			Tl_3^-		
MO sets	$^1A_1'$	$^3B_2$	$^5A_2''$	$^1A_1'$	$^3B_2$	$^5A_2''$
Ψ_σ	0.48	0.52/0.46	0.40	0.21	0.27/0.15	0.20
Ψ_π	0.33	0.29/0.38	0.16	0.32	0.32/0.29	0.17
Ψ_r	0.30	0.08/0.08	0.06	0.30	0.10/0.11	0.10
Ψ_t	−0.02	0.10/0.03	0.20	0.02	0.17/0.03	0.24

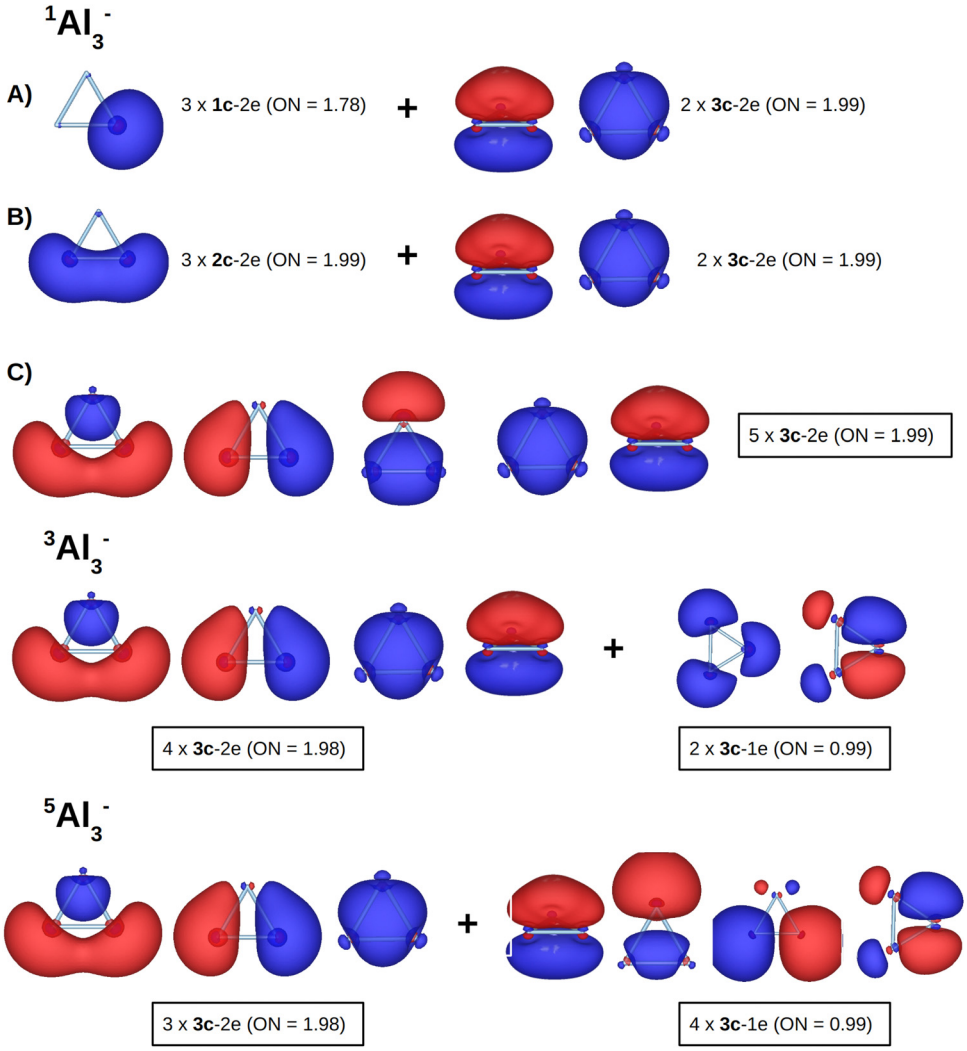

Fig. 2 AdNDP analysis of Al_3^- $^1A_1'$, $^3B_2$ and $^5A_2''$ states.

native localization schemes (A and B in Fig. 2) and the fully delocalized scheme (C in Fig. 2) suggests that there is a resonance between these solutions, reflecting the delocalized nature of the electronic density in these molecules, a fact directly related to the aromaticity. For the triplet states, we can identify the 3c–2e bonds related with the Ψ_σ and Ψ_π sets, and the 3c–1e bonds related to Ψ_r and Ψ_t sets, while for the quintets, the Ψ_σ are related with the 3c–2e bonds and the four 3c–1e bonds are related with the π-, r-sets, and the last two with the tangential sets respectively (see Fig. 2).

Finally, the iso-chemical-shielding surfaces (ICSS) method[46,47] was also used to quantify the direction and scale of the anisotropy effect (see Fig. 3). This approach can characterize aromaticity and antiaromaticity. The shielding lobes (represented in blue) surrounded by donuts like deshielding loops (represented in green) in the planar plane, describe aromatic systems, while the opposite represents an antiaromatic system. Thus, according to the ICSS, the singlet and quintet states exhibit an aromatic character, while the triplet is antiaromatic.

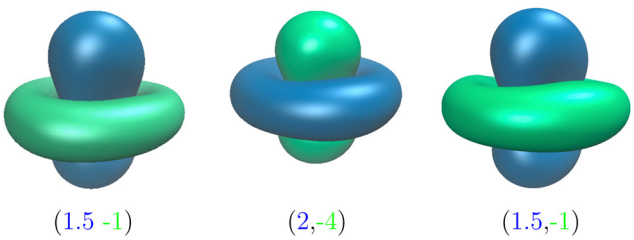

Fig. 3 ICSS plots for Al_3^- singlet, triplet, and quintet respectively. Shielding surface is shown in blue and de-shielding surfaces in green. Isovalues for the isosurfaces are shown in parentheses. The same ICSS description is found for the rest of Ga_3^-, In_3^-, and Tl_3^- triangles.

4 Discussion

After conducting a thorough analysis of the aromaticity of these structures, we have been able to rationalize it using Mandado's rules[76] who established general rules for predicting the aromaticity based on the separate α/β electron counting. Systems with $(2n + 1)$ α- (or β-) electrons are expected to be aromatic, whereas

those containing $2n$ α- (or β-) electrons are antiaromatic (n = 0, 1, 2).

In Table 3 we have summarized the outcomes after applying Mandado's rules for α and β electrons on each of the four independent MOs sets (see Fig. 1). Starting with the singlet, we have 3 α and β electrons in the Ψ_σ set, which follows Mandado's rule ($2 \times 1 + 1$) either for an α- and β-aromatic system. The σ-aromaticity of this MO set is corroborated by the MCI, DI, and AdNDP analyses shown above. The Ψ_π set is doubly occupied, thus also meets Mandado's rule ($2 \times 0 + 1$) for α and β electrons, being this set the one that provides π-aromaticity. Similarly, Ψ_r provides additional σ-aromaticity in agreement with MCI, DI, and AdNDP results. Therefore the singlets present two σ- and a π-aromatic systems, overall being an aromatic molecule which is in agreement with ICSS description (see Fig. 3).

Moving to the $^3B_2$ states, the description of the Ψ_σ and Ψ_π molecular sets is identical to that of the singlet described above. However the picture changes for Ψ_r, since now it is singly occupied with an α electron, so is the Ψ_t. We can attribute α-aromaticity to the Ψ_r, ($2 \times 0 + 1$), but we should be careful when analyzing Ψ_t. While conducting an analytical assessment, it is plausible to inadvertently apply the ($2 \times 0 + 1$) rule and consider Ψ_t aromatic, however, is crucial to note that within the tangential set, due to the odd (D_{3h}) symmetry MOs are ordered as two degenerate orbitals caped by a non-degenerate one,[77] (see Fig. 4). One of these degenerate MOs contains a single electron, being the other degenerate tangential orbital empty. Therefore, a combination of Mandado's and Baird's rules is warranted, resulting in the ($2n$) rule for aromatic compounds and the ($2n + 1$) rule for antiaromatic compounds (observe the MO orbital arrangement for odd symmetry molecules shown in Fig. 4). According to Mandado's rule extension, the Ψ_t contribution is α-antiaromatic ($2 \times 0 + 1$). Accordingly, the triplet presents what is known as conflicting aromaticity,[78] where Ψ_σ and Ψ_r present σ-aromatic contribution, the Ψ_π aromatic contributions while the Ψ_t contribution is antiaromatic. The latter contribution could explain the deshielding cones of the $^3B_2$ after applying a magnetic field (see Fig. 3). Atom-pair DIs have different values when comparing the two symmetric bonds with the third bond, in the case of Al_3^-, the $\delta_{i,j}$ corresponding to the long bond is slightly smaller than the values of the shorter bonds (1.00 *vs.* 0.92 a.u.), and this difference increases as increases the size of the atoms with values of 0.97 and 0.63 a.u. for Tl_3^-. This DI partial alternation pattern can be associated with antiaromaticity.[79] AdNDP also

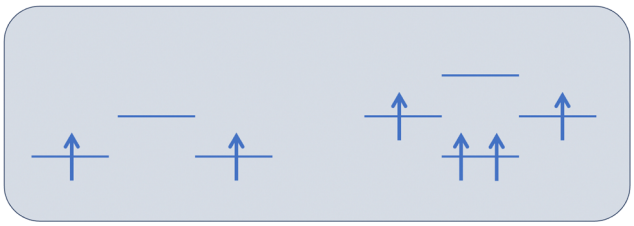

Fig. 4 Baird aromaticity representation for tangential MOs set. On the left-hand side, the arrangement corresponding to a D_{3h} odd symmetry system is shown, and the arrangement corresponding to even symmetry (D_{4h}) is on the right. Notice that Bairds classical aromaticity rule can be straightforwardly applied to even symmetry systems ($4n$) while due to the MOs rearrangement in odd symmetry systems, the Baird rule will turn into the ($2n$) rule.

agrees with the antiaromaticity description for this state. Analyzing the AdNDP objects (or bonds), we can associate one of 3c–1e objects with the radial aromaticity, which meets Mandado's aromaticity rule, and a single 3c–1e object associated to the tangential aromaticity describing an antiaromatic system for this state.

Finally, focusing on the quintets, we have the same description for the Ψ_σ as in the cases above, providing σ-aromaticity character to the molecule. The rest of the electrons are α electrons distributed as follows: one in Ψ_π and Ψ_r sets, which according to Mandado's rules, provide π-(the former) and σ-(the later) aromaticity to the system, and the last two, are in the Ψ_t set, one electron in each of the degenerate orbitals, which agrees with Baird's and Mandado's rules combination (2×1) for aromaticity. This description is in agreement with MCI (note that, though, MCI values are much smaller than those of the singlet and triplet). DI also agrees with this description, giving reasonable values for the π-, radial and tangential sets, but smaller than the singlet and triplet DIs. Finally, AdNDP reports four objects formed by one electron and three centers, where two of these centers are associated with the tangential set, thus are α-Baird aromatic, and the other two sets are describing α π- and α σ-aromaticity.

Comparing the aromaticity of the different compounds, we can say that it reduces when increasing the size of the atom, but still, we can state that the $^5A_2''$-Tl_3^- molecule exhibits some degree of aromaticity, albeit significantly lower compared to the $^1A_1'$-Tl_3^-. However, the high-spin $^5A_2''$ state is the lowest in energy for Tl_3^-, and its photo-electron spectra matches the experimental spectra available for Tl_3^-. Surprisingly, the stability of this state contradicts the conventional belief that higher

Table 3 The number of (α/β) electrons of each set is shown, and its aromaticity (A)/antiaromaticity (AA) outcomes after applying Mandado's rules to each of the four independent MOs sets. σ/π stand for the corresponding aromaticity type

Multiplicity		Ψ_σ	Ψ_π	Ψ_r	Ψ_t	Summary
$^1A_1'$	(α or β)	3 (σA)	1 (πA)	1 (σA)	0	2 × σA, πA
$^3B_2$	α	3 (σA)	1 (πA)	1 (σA)	1 (σ Baird AA)	2 × σA, πA, σ Baird AA
	β	3 (σA)	1 (πA)	0	0	σA, πA
$^5A_2''$	α	3 (σA)	1 (πA)	1 (σA)	2 (σ Baird A)	2 × σA, σ Baird A, πA
	β	3 (σA)	0	0	0	σA

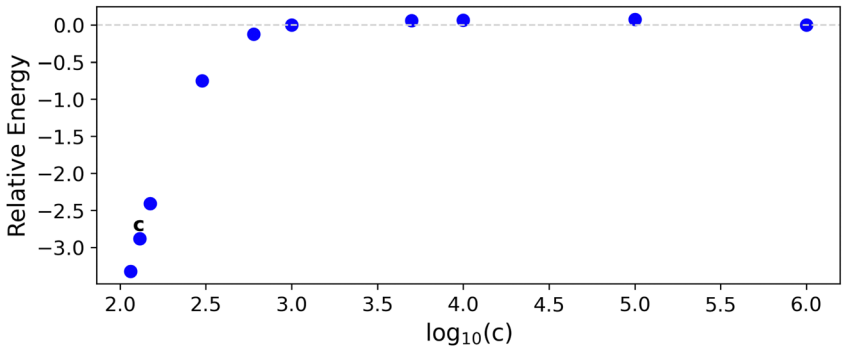

Fig. 5 Relative Energy change of Tl_3^- $\left(E(^5A_1'') - E(^1A_1'),\ \text{in kcal mol}^{-1}\right)$ with respect to logarithm of the speed of the light (in a.u.) used in the relativistic calculations. Note that the point corresponding to the real speed of the light ($\log_{10}$(137.0359895)) is indicated with a c label.

aromaticity leads to increased stability, as the singlet state is considerably more aromatic than the quintet. Despite different indicators also suggest that the quintet state is aromatic, its aromaticity remains inferior to that of the singlet state. The stability of the quintet could be attributed to the relativistic effects present in the Tl_3^- molecule, which equalize the a_2'', a_1', and both degenerate e′ orbitals in energies. As a consequence of this stabilization, are then filled up according to Hund's rule, with one electron each, being the relativistic effects more important than the stability provided by the aromaticity in the singlet state. Previous studies by Pino-Rios *et al.*[80] have also reported a loss of aromaticity due to relativistic effects, although they attributed it to spin–orbit coupling. However, the spin–orbit coupling for the Tl_3^- triangles under investigation was found to be relatively small (less than 5 cm^{-1}).

To account for the relativistic effects, the Tl_3^- $^1A_1'$ and $^5A_5''$ states where recalculated at the MCSCF (10,12) level of theory incorporating dynamic correlation through CASPT2, and employing the zeroth-order regular approximated (ZORA)[81] method with the SARC-ZORA-TZVPP[82] basis set as implemented in ORCA.[83] The geometries obtained with ZORA closely resemble the previous ones, with bond lengths of 3.147 and 3.282 Å for the singlet and the quintet respectively, the singlet being 2.91 kcal mol^{-1} higher in energy.

We conducted additional calculations by modulating the relativistic effects, altering the value of the speed of the light used in the ZORA Hamiltonian (note that increasing the speed of the light value in the Hamiltonian reduces the relativistic effects). These effects are clearly depicted in Fig. 5. As the speed of light is increased to larger values, the energy difference between the two states diminishes. When the speed of light is increased sufficiently, to the point where relativistic effects are neglected, both states become nearly energetically degenerated, indicating that relativistic effects favor the quintet with respect to the singlet.

5 Conclusions

High-level *ab-initio* quantum mechanics calculations have been performed to characterize the lowest-lying states of the X_3^- triangles, X = Al, Ga, In, and Tl.

We have assign to $^5A_2''$-Tl_3^- and to $^1A_1'$-In_3^- the experimental signals detected by Gausa *et al.* back in 1990, and we attribute the stability of the $^5A_2''$-Tl_3^- to relativistic effects.

Analyzing the electronic structures of these triangular structures, and applying Mandado's aromaticity/antiaromaticity rules, we have been able to rationalize the aromaticity of these molecules, which are in agreement with the different electron density methods employed (MCI, DI, and AdNDP) and the ICSS, which represents the response of the molecule to a external magnetic field of the molecule. The separate analysis of the α and β-electrons made possible to explain the antiaromatic character (the deshielding cone in the ICSS) of the $^3B_2$ as a consequence of the single α electron present in the Ψ_t orbital set.

Summarizing, the $^1A_1'$ electronic states present multiple-fold aromaticity, specifically 3-fold aromaticity, being the origin the Ψ_σ and Ψ_r sets, providing σ-aromaticity, and the Ψ_π which provides π-aromaticity to all the studied singlet states. The triplets are π-aromatic but they do also present certain σ-aromaticity, originated from the inner Ψ_σ and the α electron present in the Ψ_r. However, the antiaromatic character of the α electron in the Ψ_t causes a magnetic shielding/deshielding response associated with an antiaromatic system, as reported by ICSS. The quintets also present some aromatic character, which despite being smaller than that of the singlet and triplet, it is not negligible. According to Mandado's rules, the Ψ_σ set is α/β σ-aromatic, the Ψ_π set α π-aromatic, and the Ψ_t set α σ-Baird aromatic, in agreement with the diamagnetic response of the quintet.

Conflicts of interest

There are no conflicts to declare.

Acknowledgements

The authors thank for technical and human support provided by IZO-SGI (SGIker) of UPV/EHU and European funding (ERDF and ESF) and the DIPC. Financial support comes from Eusko Jaurlaritza (Basque Government) through the project IT588-22 and from Grant No. PID2020-114754GAI00 provided by

MCIN/AEI/10.13039/501100011033. The authors thankfully acknowledge also the computer resources at MareNostrum and the technical support provided by the Barcelona Supercomputing Center (Grant No. QHS-2022- 2-002 and QHS-2022-3-0015). E. M. acknowledges funding from Agencia Española de Investigación, "FEDER Una manera de hacer Europa" (PID2022-140666NB-C21), the Donostia International Physics Center (DIPC-INV-003132) and Eusko Jaurlaritza (PIBA_2023_1_0055). Open Access funding provided by University of Basque Country (UPV/EHU).

References

1 H. Basch, *Chem. Phys. Lett.*, 1987, **136**, 289–293.
2 P. Calaminici, N. Russo and M. Toscano, *Z. Phys. D – Atoms Mol. Clust.*, 1995, **33**, 281–288.
3 K. K. Baeck and R. J. Bartlett, *J. Chem. Phys.*, 1998, **109**, 1334–1342.
4 S. R. Miller, N. E. Schultz, D. G. Truhlar and D. G. Leopold, *J. Chem. Phys.*, 2009, **130**, 024304.
5 P. W. Villalta and D. G. Leopold, *J. Chem. Phys.*, 2009, **130**, 024303.
6 T. H. Upton, *Phys. Rev. Lett.*, 1986, **56**, 2168–2171.
7 M. F. Jarrold, J. E. Bower and J. S. Kraus, *J. Chem. Phys.*, 1987, **86**, 3876–3885.
8 S. Li, R. J. Van Zee and W. Weltner, *Chem. Phys. Lett.*, 1996, **262**, 298–302.
9 G. Pacchioni, P. Fantucci and J. Koutecký, *Chem. Phys. Lett.*, 1987, **142**, 85–91.
10 J. Tse, *J. Mol. Struct. THEOCHEM*, 1988, **165**, 21–35.
11 K. J. Taylor, C. L. Pettiette, M. J. Craycraft, O. Chesnovsky and R. E. Smalley, *Chem. Phys. Lett.*, 1988, **152**, 347–352.
12 G. Ganteför, M. Gausa, K. H. Meiwes-Broer and H. O. Lutz, *Z. Phys. D – Atoms Mol. Clust.*, 1988, **9**, 253–261.
13 A. E. Kuznetsov and A. I. Boldyrev, *Struct. Chem.*, 2002, **13**, 141–148.
14 C. G. Zhan, F. Zheng and D. A. Dixon, *J. Am. Chem. Soc.*, 2002, **124**, 14795.
15 J. M. Mercero, E. Matito, F. Ruipérez, I. Infante, X. Lopez and J. M. Ugalde, *Chem. – Eur. J.*, 2015, **21**, 9610–9614.
16 J. M. Mercero, R. Grande-Aztatzi, J. M. Ugalde and M. Piris, *Advances in Quantum Chemistry*, Elsevier, 2023, p. S0065327623000217.
17 B. Gerke and R. Pöttgen, *Z. Naturforsch., B: J. Chem. Sci.*, 2014, **69**, 121–124.
18 S. Seidel, R. D. Hoffmann and R. Pöttgen, *Monatsh. Chem.*, 2014, **145**, 1043–1049.
19 B. Gerke, R. D. Hoffmann and R. Pöttgen, *Z. Anorg. Allg. Chem.*, 2013, **639**, 2444–2449.
20 B. Gerke, A. Korthaus, O. Niehaus, F. Haarmann and R. Pöttgen, *Z. Naturforsch., B: J. Chem. Sci.*, 2016, **71**, 567–577.
21 S. Seidel and R. Pöttgen, *Z. Kristallogr. – Cryst. Mater.*, 2020, **235**, 53–57.
22 R. Pöttgen, *J. Alloys Compd.*, 1995, **226**, 59–64.
23 R. Pöttgen, R.-D. Hoffmann and G. Kotzyba, *Z. Anorg. Allg. Chem.*, 1998, **624**, 244–250.
24 M. F. Zumdick, G. A. Landrum, R. Dronskowski, R. D. Hoffmann and R. Pöttgen, *J. Solid State Chem.*, 2000, **150**, 19–30.
25 O. Sichevych, Y. Prots, W. Schnelle, M. Schmidt and Y. Grin, *Z. Kristallogr. – New Cryst. Struct.*, 2006, **221**, 263–264.
26 F. Haarmann, Y. Prots, S. Göbel and H. G. von Schnering, *Z. Kristallogr. – New Cryst. Struct.*, 2006, **221**, 257–258.
27 M. Wagner, R. Cardoso-Gil, N. Oeschler, H. Rosner and Y. Grin, *J. Mater. Res.*, 2011, **26**, 1886–1893.
28 X.-W. Li, W. T. Pennington and G. H. Robinson, *J. Am. Chem. Soc.*, 1995, **117**, 7578–7579.
29 Y. Xie, P. R. Schreiner, H. F. Schaefer, X. W. Li and G. H. Robinson, *J. Am. Chem. Soc.*, 1996, **118**, 10635–10639.
30 G. H. Robinson, *Acc. Chem. Res.*, 1999, **32**, 773–782.
31 N. Wiberg, T. Blank, K. Amelunxen, H. Nöth, J. Knizek, T. Habereder, W. Kaim and M. Wanner, *Eur. J. Inorg. Chem.*, 2001, 1719–1727.
32 K. Balasubramanian and P. Feng, *Chem. Phys. Lett.*, 1988, **146**, 155–161.
33 U. Meier, S. D. Peyerimhoff and F. Grein, *Z. Phys. D – Atoms Mol. Clust.*, 1990, **17**, 209–224.
34 G. Li, L. Meng, H. Zhang, X. Li and Y. Zeng, *Phys. Chem. Chem. Phys.*, 2020, **22**, 18071–18077.
35 P. Y. Feng and K. Balasubramanian, *Chem. Phys.*, 1989, **138**, 89–98.
36 M. Gausa, G. Ganteför, H. O. Lutz and K. H. Meiwes-Broer, *Int. J. Mass Spectrom. Ion Processes*, 1990, **102**, 227–237.
37 W.-Q. Zhang, G.-F. Zhao, J.-M. Sun, L.-L. Zhi and Y.-Z. Gu, *Chem. Phys.*, 2009, **361**, 44–48.
38 S. Shi, Y. Liu, Y. Li, B. Deng, C. Zhang and G. Jiang, *Comput. Theor. Chem.*, 2016, **1079**, 47–56.
39 C. Y. Cha, G. Ganteför and W. Eberhardt, *J. Chem. Phys.*, 1994, **100**, 995–1010.
40 M. Vijayakumar and K. Balasubramanian, *J. Chem. Phys.*, 1992, **97**, 7474–7488.
41 S. Kang, *Bull. Korean Chem. Soc.*, 1993, **14**, 191–195.
42 A. C. Tsipis, I. G. Depastas and C. A. Tsipis, *Symmetry*, 2010, **2**, 284–319.
43 X. Fradera, M. A. Austen and R. F. W. Bader, *J. Phys. Chem. A*, 1999, **103**, 304–314.
44 E. Matito, M. Solà, P. Salvador and M. Duran, *Faraday Discuss.*, 2006, **135**, 325–345.
45 D. Y. Zubarev and A. I. Boldyrev, *Phys. Chem. Chem. Phys.*, 2008, **10**, 5207–5217.
46 S. Klod and E. Kleinpeter, *J. Chem. Soc., Perkin Trans. 2*, 2001, 1893–1898.
47 Z. Liu, T. Lu and Q. Chen, *Carbon*, 2020, **165**, 468–475.
48 A. C. Wahl and G. Das, in *Methods of Electronic Structure Theory*, ed. H. F. Shaefer, III, Plenum Press, New York, 1977.
49 H. Nakano, *J. Chem. Phys.*, 1993, **99**, 7983–7992.
50 D. Rappoport and F. Furche, *J. Chem. Phys.*, 2010, **133**, 134105.
51 F. Weigend and R. Ahlrichs, *Phys. Chem. Chem. Phys.*, 2005, **7**, 3297.

52 B. Metz, H. Stoll and M. Dolg, *J. Chem. Phys.*, 2000, **113**, 2563–2569.
53 B. Metz, M. Schweizer, H. Stoll, M. Dolg and W. Liu, *Theor. Chim. Acta*, 2000, **104**, 22–28.
54 H. A. Witek, Y. Choe, J. P. Finley and K. Hirao, *J. Comput. Chem.*, 2002, **23**, 957–966.
55 G. M. J. Barca, C. Bertoni, L. Carrington, D. Datta, N. De Silva, J. E. Deustua, D. G. Fedorov, J. R. Gour, A. O. Gunina, E. Guidez, T. Harville, S. Irle, J. Ivanic, K. Kowalski, S. S. Leang, H. Li, W. Li, J. J. Lutz, I. Magoulas, J. Mato, V. Mironov, H. Nakata, B. Q. Pham, P. Piecuch, D. Poole, S. R. Pruitt, A. P. Rendell, L. B. Roskop, K. Ruedenberg, T. Sattasathuchana, M. W. Schmidt, J. Shen, L. Slipchenko, M. Sosonkina, V. Sundriyal, A. Tiwari, J. L. Galvez Vallejo, B. Westheimer, M. Wloch, P. Xu, F. Zahariev and M. S. Gordon, *J. Chem. Phys.*, 2020, **152**, 154102.
56 P. Bultinck, R. Ponec and S. Van Damme, *J. Phys. Org. Chem.*, 2005, **18**, 706–718.
57 E. Matito, ESI-3D: Electron Sharing Indices Program for 3D Molecular Space Partitioning, 2006, **https://ematito.dipc.org/programs.html**.
58 P. Salvador and E. Ramos-Cordoba, *APOST-3D Program*, 2014, Institut de Química Computacional i Catàlisi. Universitat de Girona (Spain).
59 I. Mayer and P. Salvador, *Chem. Phys. Lett.*, 2004, **383**, 368–375.
60 P. Salvador and E. Ramos-Cordoba, *J. Chem. Phys.*, 2013, **139**, 071103.
61 A. D. Becke, *J. Chem. Phys.*, 1988, **88**, 2547–2553.
62 T. Lu and F. Chen, *J. Comput. Chem.*, 2012, **33**, 580–592.
63 A. P. Sergeeva, B. B. Averkiev and A. I. Boldirev, in *Metal–Metal Bonding*, ed. G. Parkin, Springer-Verlag, Berlin, Germany, 2010, vol. 136 of Structure and Bonding, pp. 275–306.
64 J. M. Mercero, I. Infante and J. M. Ugalde, in *Aromaticity and Metal Clusters*, ed. P. K. Chattaraj, CRC Press, Boca Raton, FL, USA, 2011, ch. 16, pp. 323–337.
65 J. V. Ortiz, *J. Chem. Phys.*, 1996, **104**, 7599–7605.
66 M. J. Frisch, G. W. Trucks, H. B. Schlegel, G. E. Scuseria, M. A. Robb, J. R. Cheeseman, G. Scalmani, V. Barone, G. A. Petersson, H. Nakatsuji, X. Li, M. Caricato, A. V. Marenich, J. Bloino, B. G. Janesko, R. Gomperts, B. Mennucci, H. P. Hratchian, J. V. Ortiz, A. F. Izmaylov, J. L. Sonnenberg, D. Williams-Young, F. Ding, F. Lipparini, F. Egidi, J. Goings, B. Peng, A. Petrone, T. Henderson, D. Ranasinghe, V. G. Zakrzewski, J. Gao, N. Rega, G. Zheng, W. Liang, M. Hada, M. Ehara, K. Toyota, R. Fukuda, J. Hasegawa, M. Ishida, T. Nakajima, Y. Honda, O. Kitao, H. Nakai, T. Vreven, K. Throssell, J. A. Montgomery, Jr., J. E. Peralta, F. Ogliaro, M. J. Bearpark, J. J. Heyd, E. N. Brothers, K. N. Kudin, V. N. Staroverov, T. A. Keith, R. Kobayashi, J. Normand, K. Raghavachari, A. P. Rendell, J. C. Burant, S. S. Iyengar, J. Tomasi, M. Cossi, J. M. Millam, M. Klene, C. Adamo, R. Cammi, J. W. Ochterski, R. L. Martin, K. Morokuma, O. Farkas, J. B. Foresman and D. J. Fox, *Gaussian16 Revision B.01*, 2016, Gaussian Inc., Wallingford CT.
67 M. Solà, *Front. Chem.*, 2017, **5**, 5–8.
68 G. Merino, M. Solà, I. Fernández, C. Foroutan-Nejad, P. Lazzeretti, G. Frenking, H. L. Anderson, D. Sundholm, F. P. Cossío, M. A. Petrukhina, J. Wu, J. I. Wu and A. Restrepo, *Chem. Sci.*, 2023, **14**, 5569–5576.
69 M. Solà, I. Fernández and G. Merino, *Chem. Sci.*, 2023, **14**, 9628–9629.
70 M. Giambiagi, M. S. De Giambiagi, C. D. Dos Santos Silva and A. P. De Figueiredo, *Phys. Chem. Chem. Phys.*, 2000, **2**, 3381–3392.
71 F. Feixas, E. Matito, J. Poater and M. Solà, *J. Comput. Chem.*, 2008, **29**, 1543–1554.
72 F. Feixas, E. Matito, J. Poater and M. Solà, *Wiley Interdiscip. Rev.: Comput. Mol. Sci.*, 2013, **3**, 105–122.
73 J. Cioslowski, E. Matito and M. Solà, *J. Phys. Chem. A*, 2007, **111**, 6521–6525.
74 E. Matito, *Phys. Chem. Chem. Phys.*, 2016, **18**, 11839–11846.
75 I. Casademont-Reig, E. Ramos-Cordoba, M. Torrent-Sucarrat and E. Matito, in *Aromaticity*, ed. I. Fernandez, Elsevier, 2021, pp. 235–259.
76 M. Mandado, A. M. Graña and I. Pérez-Juste, *J. Chem. Phys.*, 2008, **129**, 164114.
77 J. M. Mercero, I. Infante and J. M. Ugalde, in *Aromaticity and Metal Clusters*, ed. P. K. Chattaraj, CRC Press, Florida, 2011, ch. 16, pp. 323–338.
78 D. Chen, D. W. Szczepanik, J. Zhu and M. Solà, *Chem. Commun.*, 2020, **56**, 12522–12525.
79 F. Feixas, E. Matito, M. Solà and J. Poater, *Phys. Chem. Chem. Phys.*, 2010, **12**, 7126–7137.
80 R. Pino-Rios, A. Vásquez-Espinal, L. Alvarez-Thon and W. Tiznado, *Phys. Chem. Chem. Phys.*, 2020, **22**, 22973–22978.
81 C. van Wüllen, *J. Chem. Phys.*, 1998, **109**, 392–399.
82 D. A. Pantazis and F. Neese, *Theor. Chem. Acc.*, 2012, **131**, 1292.
83 F. Neese, *Wiley Interdiscip. Rev.: Comput. Mol. Sci.*, 2022, **12**, e1606.